SIFT DESK

Journal of Computational Chemistry & Molecular Modeling (ISSN: 2473-6260)

Investigation on Spectral properties of 3-Chloro-3'-Methoxystilbene for Anticancer Drugs Application: Using Density Functional Theory

DOI: 10.25177/JCCMM.3.2.RA.558

Research

Received Date: 08th Aug 2019
Accepted Date: 05th Oct 2019
Published Date:20th Oct 2019

A. Prakasam[b]

[a]*Department of Physics, Periyar University, Salem - 636 011, India.*

[b]*Department of Physics, Thiruvalluvar Government arts college, Rasipuram, Namakkal – 637 401, India*

CITATION

A. Prakasam, Investigation on Spectral properties of 3-Chloro-3'-Methoxystilbene for Anticancer Drugs Application: Using Density Functional Theory(2019) Journal of Computational Chemistry & Molecular Modeling 3(2) p: 294-312

ABSTRACT

The ground state optimized structure and spectroscopic analysis of 3-chloro-3'-methoxystilbene (3C3'MS) were studied experimentally by FT-IR techniques and computationally by the first principle density functional theory (DFT) and Hartree-Fock (HF) method with 6-311++G (d, p) level of theory. The computational vibrational frequencies have been assigned and they agreed satisfactorily with experimental FT-IR and FT-Raman spectra. The computed maximum wavelength of absorption of 3C3'MS are calculated in different solvents (Acetonitrile, Methanol and Ethanol) by TD-DFT method. The experimental available ^{1}H and ^{13}C nuclear magnetic resonance chemical shifts calculations have been calculated by using the Gauge independent atomic orbital (GIAO) method and compared with the computational studies. The NBO atomic charges analysis in conjunction with spectral data recognized the occurrence of intra-molecular interactions such as hyperconjugative, mesomeric and steric effects in 3C3'MS. Electronic distribution and Frontier molecular orbital energy values of 3C3'MS are discussed in terms of intra-molecular interactions. Computed values of Mulliken charges, Quantum Chemical descriptors and thermodynamic properties of 3C3'MS along with molecular electrostatic potential (MEP) are reported. Moreover, the estimation of the molecule confirms the biological behavior.

Keywords: FT-IR, FT-Raman, NMR spectra, NBO, NLO and NPA analysis, Thermodynamic properties, MEP analysis.

1. INTRODUCTION

Stilbene and its derivatives are one of the most thoroughly studied compounds from the standpoint of mechanistic and preparative photochemistry [1-5]. The importance of the ring closure reaction channel in cis and trans-stilbene was recognized early [6] and most in recent time's stilbene has become a prototype for ultrafast studies of photoisomerization [7-10]. The importance of stilbene photochemical analogous studies has been performed for only a limited range of stilbene and its derivatives. Our final goal is to obtain a clearer picture of the effect of different solvents and substituents on photochemical processes for cis and trans-stilbene derivatives. In these derivatives are important oligomeric compounds with a broad range of biological action, including hormonal, hypocholesterolemic, Sympathomimetic, antifungal, antiallergic, Human hemoglobin, antibacterial, antimalarial, Human serum albumin and anticancer activity. 3-chloro-3'-methoxystilbene are very important bioactive molecule [11-14]. The most famous stilbene derivatives, which was used medically for prostate and breast cancer, and to prevent threatened abortions [15-18]. Seigo sanoh et al. reported the trans-stilbene is metabolically activated to estrogenic compounds by liver microsomal enzyme molecular system. The physical requirement for estrogenic activity of different stilbene derivatives (Cis and Trans) including proestrogens [19]. Kyosuke Tsumura et al. reported DFT and TD-DFT, together with the analytical calculation of numerical and gradients calculation of the Hessian matrix has been applied to calculate the FT-IR, FT-Raman and fluorescence excitation spectrum of trans-stilbene (tSB) in the lowest excited singlet (S1) state [20]. The Excited-state reduction of cis-stilbene and trans-stilbene is outlined with femtosecond computed FT-Raman spectroscopy, using $S_n \rightarrow S_1$ resonance conditions. For isomers, decay in FT-Raman shift, intensity of spectral positions and mind broadening of the bands specify IVR. In n-hexane this process effectively takes 0.5-0.7 ps [21]. Rajat K. Chaudhuri et al. reported Molecular geometries are calculated for the ground state and excited states of 4a,4b-dihydrophenanthrene (DHP), cis-stilbene, and trans-stilbene from calculations accomplished with the developed fundamental orbital, complete active space configuration intermolecular interaction (IVO-CASCI) method. The calculations indicate that a non-planar conformer of tSB is the most stable between the photoisomers [22].The photoisomerization dynamics of tSB have been well studied in the lowest excited state, but much less is known about the performance following excitation to higher excited states. This contribution reports a combined study of the spectroscopy and dynamics of two-photon available states above S1. Two-photon absorption (2PA) measurements using a broadband pump−probe technique reveal distinct bands near 5.1 and 6.4 eV are reported by Amanda L. Houk et al [23].

Nowadays, Modern vibrational spectroscopy has become a very popular analytical technique for solving many chemical problems. This is especially true of studies using Raman spectroscopy is a powerful technique, which gives information about the vibrations modes of the atoms and molecular structure, specific information on various chemical composition and Fourier transform infrared spectroscopy (FT-IR) is as an analytical method to identification of the functional groups, the degree of conjugation and interaction with drugs. The problem of signal vibrations however, as well as understanding the relationship between the observed vibration spectra and molecule structure, and chemical reactivity can be difficult. Even identification of important vibrational modes often generates controversy [24]. Recently, computational technique and DFT is an advance quantum chemical approach that plays an important role in the understanding of molecular system, vibrational spectrum and of the various properties of biological activity [25-28]. In particular for polyatomic molecules the quantum chemical method lead to the calculation of the more perfect molecular system and vibrational Spectrum (Infrared and Raman spectroscopies) than the conventional ab initio RHF and MP2 method [24] and the three-parameter B3LYP density functional, which includes Becke's gradient exchange correction [29] and the Lee-Yang-Parr correlation functional [30].

In previous work, we wish to report the experimental and theoretical investigation of vibrational spectral analysis and ground state geometric structure of this

bioactive 3-Chloro-3'-Methoxystilbene molecule and their results have been discussed. Moreover, the calculated vibrational wavenumber of potential energy distribution (PED) was assigned and Molecular Electrostatic Potential (MEP) map of title compound has been reported. The HOMO-LUMO energy gap to supports to pharmacological active property and Natural bond orbital (NBO) charge analysis has been performed to investigate charge transfer interactions and the hydrogen bonding within the molecule. The electronegativity, chemical hardness and softness values were also considered by utilizing frontier molecular orbital energy gaps of title compound.

2. MATERIALS & METHODS

2.1. Experimental Details

This chemical with a purity of 99% is purchased form Alfa Aesar chemical suppliers (India) and were used as received. FT-IR measurements were performed using Mattson 1000 FT-IR spectrometer in the 4000 and 400 cm^{-1} region. The FT-Raman spectrum of 3C3'MS was recorded between the region 4000 and 50 cm^{-1} using a Bruker FRA 106/S FT-Raman instrument using 1064 nm excitation from an Nd: YAG laser. The detector used was a liquid nitrogen cooled Ge detector. ^{1}H NMR and ^{13}C NMR spectrum was recorded at 400 MHZ on BRUKER AV-III 400 MHZ instruments.

2.2. Computational details

The theoretical calculations were performed using the Gaussian 09 program package [31]. The optimized geometries were obtained employing DFT and HF [32, 33] functional in conjunction with 6-311++G (d, p) basis set. Subsequently, the vibrational IR and Raman spectra were calculated at harmonic approximation. All the calculated computed harmonic frequencies were real, which confirm that the optimized structures correspond to minimum energies. The internal coordinates of the molecule were converted to the local symmetry coordinates. The distributions of assignment of the computed wavenumbers have been aided by means of MOLVIB-7.0 program [34, 35]. The Cartesian representation of the force constants were transferred to a non-redundant set of symmetry coordinates, internal coordinate system recommended by Pulay et al. [36] is used for the assignment of vibrational modes. All the molecular structures are pictured using software Gauss-view [37]. ^{1}H and ^{13}C NMR isotropic shielding were calculated by GIAO method using optimized parameters obtained from DFT/6-311++G (d, p) method. The electronic properties such as oscillator strengths of electronic singlet-singlet transitions, absorption wavelengths and calculate energies were determined by TD-DFT method and Hence, the HOMO and LUMO energies and chemical hardness, softness, electrophilicity index and electronegativity were assumed from electron affinity and ionization potential have also been evaluated in the present study.

3. Results and discussion

3.1 Molecular Geometry

The most optimized geometrical parameters such as, bond lengths, bond angles and dihedral angles of title compound calculated at initio DFT and HF methods with 6-311++G(d,p) level of theory and optimized structure of the host molecule along with numbering scheme in Fig. 1. The calculated bond lengths between C12-C2, C5-Cl17 in DFT and HF methods are found to be 1.3514, 1.3315 Å and 1.8309, 1.8117 Å respectively. The bond angle between C5-C4-20 in HF and DFT are 120.0677 and 119.6667^{o} respectively in Fig. 2b.The dihedral angle between C8-C3-C4-H20 in HF and DFT are 180.001^{o} and 179.9987^{o} respectively. The Computed geometrical parameters can be used to determine the other parameters of 3C3'MS. The bond lengths, bond angles and dihedral angles were referred from [38]. Fig.2. Graphical representation of correlation coefficient and linear relationships of between the DFT and HF bond lengths, bond lengths and dihedral angles were determined for 6-311++G(d,p) basis set.

The optimized bond lengths of C-H in methyl ring in calculated range from 1.0893, 1.0965, 1.0965 Å and 1.0762, 1.0823, 1.0823 Å for 3C3'MS. The C-H bond angles are found 109.7164, 109.6621, 109.7152 and 109.6616, 109.5451, 109.7381 Å for 3C3'MS respectively, from DFT and HF/6-311++G (d, p) methods, which are in good agreement with calculated values for C-H bond lengths and bond angles of methyl ring.

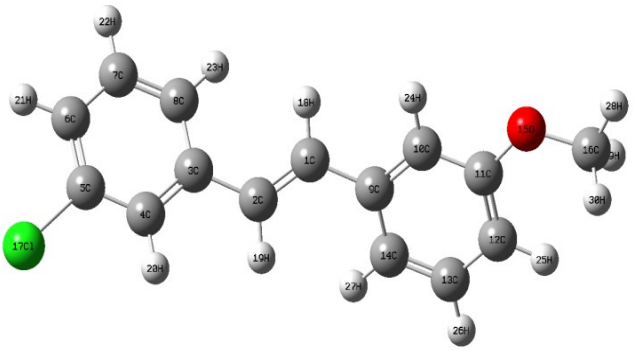

Fig. 1 Optimized geometrical structure

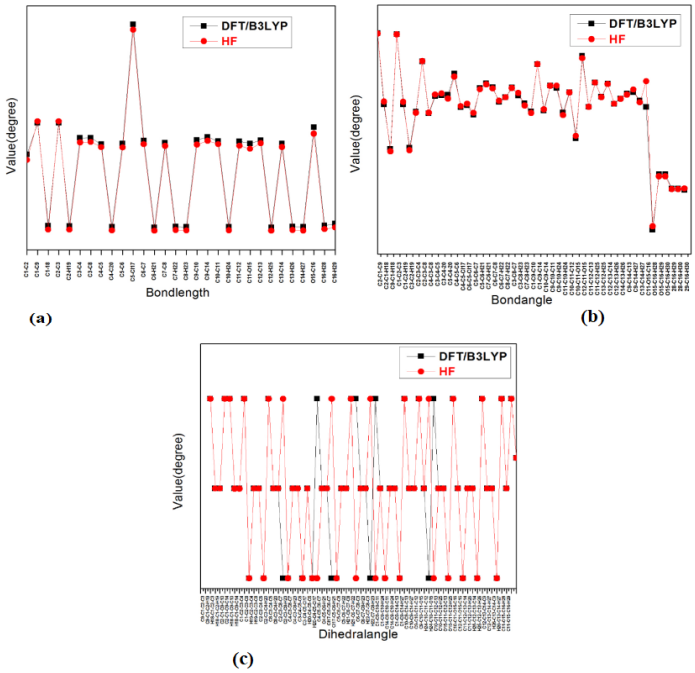

Fig. 2 Bond lengths, bond angles and dihedral angles differences between DFT and HF approaches

4.2 HOMO-LUMO energy gap

Frontier molecular orbitals (FMOs) play a major role in the kinetic stability or molecular chemical reactivity and the interactions between atoms. They are measured to be effective in determining the characteristics of the molecule such as pharmaceutical and biological activities. The organic molecule containing conjugated π electrons characterized by a small HOMO-LUMO separation energy, which is the result of a significant degree of Intramolecular change transfer (ICT) from the end-capping electron donor groups to the efficient electron acceptor groups through conjugated path [39]. The calculated HOMO-LUMO energy gap of the title molecule is -4.17 eV at the B3LYP level, respectively. The Large energy gap is basically a significance of the large stabilization of the LUMO due to the strong electron−accepting ability of the electron−acceptor group. The graphical diagram of HOMO and LUMO orbitals and their respective positive and negative regions are shown in Fig. 3. Such a plot suggests that in the HOMO → LUMO excitation the benzene ring π electrons are transferred to chloride group. The chemical reactivity of organic molecules such as chemical hardness and softness can be calculated from HOMO and LUMO energy gap values. The atomic π-orbital's point towards each other and an increase in π-character points the fact that σ-bonds are stronger as showed by natural bond analysis. A highly delocalized LUMO indicates that the electrons can more readily move around the molecule from HOMO-LUMO and hence an improved ICT [40] shown in Table 1. The HOMO electrons are mostly localized on the methyl group attached to the benzene ring while LUMO is mainly delocalized on the benzene ring indicating the presence of favorable atomic center within 3C3'MS for possible nucleophile attacks(hydrogen bond acceptor) revealing its bioactivity. Both the HOMO and LUMO are mainly localized around the two benzene rings which show that they are π type orbitals. There are lots of applications available for the use of HOMO and LUMO energy gap as a computational calculation.

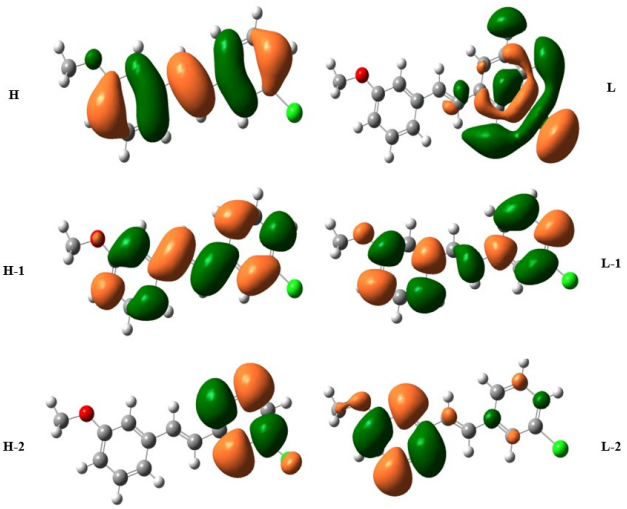

Fig. 3 Schematic view of the important Molecular Orbitals of TD-DFT/6-311++G (d, p) method.

Table 1. Molecular Properties end energy gap (eV) between molecular orbitals involved in electronic transitions of 3C3'MS.

Global Activity	DFT	Acetonitrile	Ethanol
HOMO (eV)	5.77	5.93	5.97
LUMO (eV)	1.6	1.74	1.51
Energy gap(eV)	4.17	4.19	4.46
Hardness (η)	2.08	2.09	2.23
softness (S)	0.240	0.239	0.224
Ionization potential (μ)	-3.68	-3.83	-3.74
Electronegativity (χ)	3.68	3.83	3.74
Electrophilicity index (ω)	3.233	3.509	3.136

4.3 Vibrational analysis

The vibrational spectral analysis is to end vibrational frequencies connected with specific molecular structures of calculated title molecule. The normal vibrations are distributed as 56A'+31A" considering C_s symmetry. All the 87 normal modes of vibrations are active in both IR and Raman. Vibrational wavenumber was calculated using the DFT and HF methods with the single split valence basis set 6-311++G (d, p). Table 3 the vibrational assignments in the present study are based on the scaled wavenumbers DFT and HF/6-311++G (d, p) vibrational frequencies, Reduced Mass, Raman activity, IR intensities, Depolarization Ratio, Force Constants and fundamental modes descriptions (characterized by PED) of the title compound. The comparison between the observed frequencies and the computational FT-IR and Raman spectra support each other. Including of electron correlation in computational theory to a certain extend makes the frequency values smaller in comparison with the HF frequency data. All frequency modes are active both in IR and Raman Spectra. For this purpose, the full set of 87 normal internal coordinates and description of vibrational assignments of fundamental modes can be given by means of normal coordinates have been reported in Table 2. The calculated and experimental of FT-IR [41], FT-Raman spectra are shown in Figs. 4 and 5.

Table 2 Definition of internal coordinates of 3C3'MS.

No (i)	Symbol	Type	Definition
Stretching			
1-15	r_i	C-C	C1-C2, C2-C3, C3-C4, C4-C5, C5-C6, C6-C7, C7-C8, C8-C3, C1-C9, C9-C10, C10-C11, C11-C12, C13-C14, C14-C9
16-25	R_i	C-H (Ring)	C1-H18, C2-H19, C4-H20, C6-H21, C7-H22, C8-H23, C10-H24, C12-H25, C13-H26, C14-H27
26-28	R_i	C-H (methyl)	C16-H28, C16-H29, C16-H30
29	P_i	C-CI	C5-CI17
30-31	Q_i	C-O	C11-O15,C16-O15
Bending			
32-43	a_i	C-C (Ring)	C3-C4-C5, C4-C5-C6, C6-C7-C8, C7-C8-C3, C8-C3-C4, C9-C10-C11, C10-C11-C12, C11-C12-C13, C12-C13-C14, C13-C14-C9, C14-C9-C10
44-46	b_i	C-C-C	C9-C1-C2, C1-C2-C3, C2-C3-C4
47-48	b_i	C-C-C	CI17-C5-C4, CI17-C5-C6
49-51	b_i	H-C-H	H28-C16-H29, H29-C16-H30, H30-C16-H29
52-54	b_i	O-C-H methyl	O15-C16-H28, O15-C16-H29, O15-C16-H30
55-65	j_i	C-C-H	C3-C4-H20, C5-C6-H21, C6-C7-H22, C7-C8-H23, C2-C3-H19, C2-C1-H18, C9-C14-H27, C13-C14-H26, C13-C12-H25, C11-C10-H24, C9-C1-H18
66	b_i	C-O-C	C11-O15-C16
67-68	b_i	C-C-O	C12-C11-O15, C10-C11-O15
Out-of-plane bending			
69-76	ω_i	C-H (Ring)	H20-C4-C5-C6, H21-C5-C6-C7, H22-C6-C7-C8, H23-C7-C8-C3, H24-C9-C10-C11, H25-C11-C12-C13, H26-C12-C13-C14, H27-C9-C14-C13
77	ω_i	C-O	C12-C11-O15-C16
Torsion			
78-81	τ_i	τ C-C Ring	C3-C4-C5-C6, C4-C5-C6-C7, C5-C6-C7-C8, C6-C7-C8-C3
82-84	τ_i	τ C-CH_3	(C12)C11-C15-C16-H28, (C12)C11-C115-C16-H, (C12)C11-C15-C16-H30
85	τ_i	τ CI-C	CI-C4-C5-C6
86-87	τ_i	τ C-H	H20-C4-C5-CI17, H21-C6-C5-CI17

Table 3. Experimental Theoretical harmonic frequencies (cm^{-1}) of the 3C3'MS molecule along with the assignments of vibrational modes basing on PED results.

S.no	Experimental Wavenumber (cm^{-1})		Scaled Wavenumber (cm^{-1})			IR Intensty (A_i)	Raman active (I_i)	Depolarisation Ratio	Reduced Mass (μ)	Force Constants (K)	Assignments with PED (%)
	FT-IR	FT-Raman	DFT	HF	d_{IR-Ra}						
	-	-	3295	3247	48	3.8458	172.844	0.7472	1.092	6.8043	νCH(99)
1	3182	3179	3290	3241	49	14.805	158.127	0.75	1.0924	6.7681	β_{ipd} CH_3(98)
2	3153		3278	3228	50	1.395	106.788	0.75	1.0906	6.7088	β_{ipd} CCC(391)
3	3089	3160	3276	3226	50	16.675	12.2342	0.2055	1.092	6.6998	δCH_3(91)
4	3060	3053	3275	3225	51	9.6079	71.0921	0.1788	1.0924	6.6952	τRCCCC(90)
5	-	3011	3270	3221	49	7.7395	24.6103	0.3838	1.0906	6.6696	νCH(32), ν^1CH(89)
6	3015	-	3252	3205	47	8.9023	73.4806	0.3243	1.0872	6.5837	τCOCC(87)
7	3001	2996	3245	3199	46	9.094	71.0542	0.4637	1.0873	6.5567	β_{ipd} CH_3(86)
8	-	2989	3222	3181	41	22.978	150.064	0.4767	1.0987	6.5505	νCH(86)
9	-		3215	3176	39	38.311	2.7141	0.4785	1.0855	6.4538	νCH(86)
10	-	-	3214	3166	48	1.6292	39.3106	0.4782	1.0904	6.4432	ν OC(81)
11	2995	2816	3142	3103	39	44.149	70.5652	0.5042	1.1045	6.2681	νCH(70)
12	2985	2791	3078	3032	46	56.836	163.546	0.2039	1.0334	5.6011	νCH(71)
13	2883	2650	2824	2710	114	5.0391	3601.83	0.3949	5.0901	8.7782	νCH(69)
14	2690	2612	2773	2754	19	124.41	560.612	0.75	6.0364	9.8682	νCH(45), νCH(59)
15	-	-	1763	1665	98	21.466	2728.8	0.0358	5.7656	9.2794	ν CH(59)
16	-	1937	1737	1652	85	100.03	607.442	0.327	4.8112	7.5584	ν CH(68), νCH(59)
17	-	-	1722	1632	90	36.787	21.835	0.3694	5.2171	8.0186	τRCCCC(45)
18	-	1823	1678	1615	63	47.271	76.3514	0.3699	2.1221	3.0029	τCCCC(11),τ^2CCCC(45)
19	-	-	1669	1549	120	60.334	13.9519	0.3559	1.0992	1.5445	τ_{ac} CC(43)
20	1735	-	1660	1544	116	14.089	242.346	0.3882	2.174	3.032	β_{ipd} CCC(43)
21	1712	1692	1652	1538	114	8.9211	39.0981	0.3059	1.0541	1.4578	τHCCC(10), τ^2 HCCC(43)
22	1683	-	1634	1532	102	8.9246	27.6593	0.7207	1.7797	2.3705	ν CH(40)

23	1640	1623	1600	1503	97	32.644	43.8815	0.3352	1.5431	2.0263	τ HCCC(40), τ^2 HCCC(13)
24	1610	1584	1564	1492	72	2.2286	213.605	0.75	2.7353	3.4868	β_{ipd} CCC(37), β_{ipd} CCC(14)
25	1578	1572	1508	1470	38	0.2645	241.023	0.4639	2.0129	2.3229	ν CC(33)
26	-	-	1499	1399	100	1.22	403.196	0.4473	1.7307	1.993	δHCC(33)
27	-		1480	1398	82	8.1576	41.2814	0.3305	1.9628	2.2066	ν CC(32)
28	-	-	1471	1381	90	0.3392	7.748	0.3303	1.6129	1.7843	ν CH(31), ν^2CH(19)
29	1381	1362	1398	1370	28	4.2141	28.9577	0.2924	2.1216	2.299	τ HCCC(29), τ^2 HCCC(15)
30	1342	1321	1366	1356	10	39.397	20.6353	0.5409	3.7464	3.86	δCOC(29)
31	-	-	1358	1322	36	163.97	202.851	0.6478	2.099	2.1097	δCICC(22) ,δCICC(28)
32	1318	1300	1334	1306	28	27.417	607.619	0.376	2.4642	2.3205	ν CC(23) , ν^2 CC(34)
33	1294	1285	1327	1264	63	2.1191	73.976	0.304	1.2226	1.105	ν CC(23)
34	1281	1266	1287	1238	49	1.2604	160.336	0.2754	1.1321	1.0117	ν CC(22)
34	1249	1252	1283	1231	52	48.352	323.027	0.3022	1.4881	1.2868	βHCC(18)
35	-	1235	1242	1211	31	46.428	229.473	0.4451	1.5723	1.3158	τ R2CCCC(18)
36	-	-	1231	1191	40	0.2944	9.3401	0.3076	1.2546	1.0026	τ RCCCC(39) , τ^2R CCCC(19)
37	-	1201	1213	1164	49	9.8272	1.7765	0.3179	1.6512	1.2671	δOCCC(13)
38	1215	1213	1203	1141	62	6.8866	1.659	0.3497	1.7233	1.3141	ν CH(11) , ν^2CH(13)
39	1207	1194	1198	1137	57	26.837	7.6438	0.75	2.2871	1.6696	δHCC(23) , δHCC(13)
40	-	1187	1183	1113	70	104.3	12.22	0.6135	4.369	2.8532	βHCH(23)
41	-	-	1173	1052	121	12.328	0.0492	0.353	5.9102	3.679	β_{ipd} CCC(13)
42	1172	-	1162	1027	135	1.9548	357.685	0.2176	5.7932	3.6002	τ RCCCC(22)
43	1132	1132	1123	1027	96	46.244	0.0466	0.2813	1.1466	0.709	τ HCCC(13)
44	1125	1113	1114	1008	106	4.0565	1.8511	0.75	1.3153	0.7888	βCCC(12)
45	1119	1105	1112	996	116	1.4003	0.6293	0.7498	1.3103	0.767	τ HCCC(12)
46	1089	998	1091	954	137	0.642	35.3366	0.75	1.9774	1.0614	τ RCCCC(12)
47	1081	963	1087	932	155	1.3584	0.5733	0.7497	1.3851	0.7093	βCCC(12)
48	1074	-	1083	931	152	4.8048	23.4977	0.5021	4.3495	2.2216	τ HCCC(10)

49	1071	947	1075	919	156	26.913	1.4612	0.75	1.524	0.7598	τ RCCCC()10
50	-	-	1040	905	135	4.3035	2.4844	0.7266	1.4884	0.7185	bHCC(10)
51	-	921	979	904	75	37.658	21.3403	0.5853	4.5931	2.2164	τ HCCC(11)
52	-	-	969	884	85	1.0979	7.8601	0.75	1.4935	0.6884	βCCCC(10)
53	-	907	954	815	139	52.182	1.6439	0.75	1.4915	0.584	τ HCCC (31), τ^2 HCCC(10)
54	-	-	95	805	148	20.55	4.4528	0.75	1.4961	0.5717	ν OC(11)
55	872	832	831	785	46	0.2449	10.4039	0.1385	6.2195	2.2597	ν ClC(31)
56	-	-	816	715	101	39.672	0.0327	0.7499	1.9067	0.5756	βHCC(11)
57	856	815	801	713	88	46.755	0.874	0.2464	7.2344	2.171	ν ClC (11), βHCC(34)
58	841	796	759	702	57	0.2897	0.5042	0.75	2.1704	0.631	τ HCOC(10)
59	-	721	728	677	51	0.7455	7.974	0.4293	6.6003	1.7863	ν CC(10)
60	-	682	714	628	86	0.0126	0.3703	0.75	4.6218	1.076	βHCC(10)
61	672	-	647	585	62	23.488	1.5686	0.4693	4.9281	0.9958	τ RCCCC(11)
62	643	-	633	561	72	0.2659	0.3162	0.733	4.2091	0.7813	τ HCCC(10)
63	621	583	601	560	41	11.516	0.7849	0.2804	6.5422	1.2131	ν CH(10)
64	590	545	555	515	40	0.3552	1.698	0.3608	4.6916	0.7359	ν CH (11), νCH(25)
65	-	480	546	470	76	2.7885	0.0183	0.75	3.0372	0.3968	βCCC(10)
66	515	-	530	455	75	1.4285	0.1483	0.75	2.9843	0.364	τ HCCC(12)
67	-	432	476	444	32	4.0224	16.5656	0.3067	5.2709	0.6144	ν CC(10)
68	437	413	447	424	23	5.9169	8.6724	0.2962	9.6166	0.8797	βCCC(10)
69	411	410	415	419	12	1.6465	1.9902	0.3616	4.5785	0.2761	τ CCCC(10)

ν→Stretching, β→ Bending, τ→torsion, δ→Out-of-plane bending, β_{ipd}→in-plane bending, R→ring

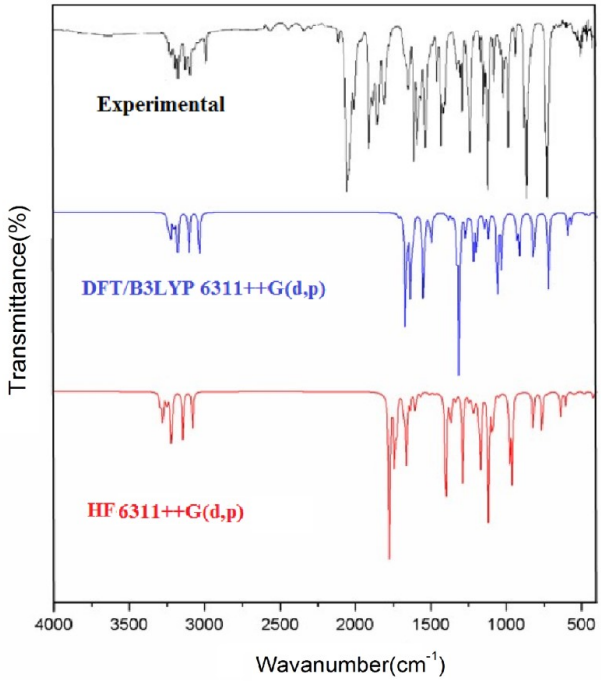

Fig. 4 Experimental and theoretical FT-IR spectra.

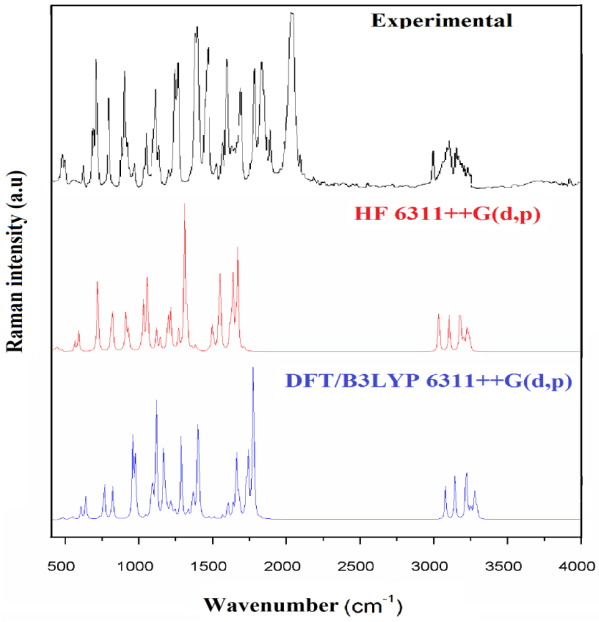

Fig. 5 Experimental and theoretical FT-Raman spectra.

4.3.1 Carbon-Hydrogen Vibrations

The C-H stretching is considered as characteristic Wavenumbers. Such differences are usually observed for C-H vibrations. The aromatic ring shows the occurrence of C-H stretching vibration modes in the range 3100-3000 cm^{-1} region [42, 43], which is the normal region for ready identification of C-H stretching vibrations. The title compounds observed C-H stretching vibration modes are assigned 3082,3053,3011,2984 cm^{-1} in FT-IR and 3079, 3060, 2983 cm^{-1}in FT-Raman spectra. The Calculated scaled DFT/6311++G (d, p) and HF Values are 3103,3032,2710,2773 cm^{-1} and 3142,3078,2824,2754 cm^{-1} have been assigned to C-H stretching vibrations respectively.

4.3.2 Methyl group Vibrations

The Methyl group vibration modes for the assignments of CH_3 group frequencies, fundamentally nine normal vibration modes can be associated to each Methyl group [44] namely, CH_3 ss– symmetric stretch, CH_3 ips– in-plane stretch , CH_3 ops – out-of-plane stretch, CH_3 ipb – in-plane bending , CH_3 opb-out-of-plane bending , CH_3 ops – out-of-plane stretch,CH_3 ipr – in-plane rocking , CH_3 opr-out-of-plane rocking; CH_3 ipb – in-plane bending, CH_3 out-of-plane bending modes, CH_3 sb–symmetric bending, tCH_3-twisting modes of CH_3 group vibrations would be predictable to be depolarized for A" symmetry species. The methyl C-H vibrations appear lower frequencies then aromatic C-H stretching vibrations. The calculated Scaled DFT and HF of in-of-plane bending and out-of-plane bending modes of CH_3 values are 3290,3276,3245 cm^{-1} and 3241,3226,3199 cm^{-1}. The observed CH_3 opb and ipb assigned 3182,3089,3001 cm^{-1} in FT-IR and 3179,3160,2996 cm^{-1} FT-Raman spectra. The CH_3 group vibrations computed DFT and HF/6311++G (d, p) methods also show good agreement with recorded spectral data.

4.3.3 Chlorine -Carbon Vibrations

The characteristic Cl-C stretching mode has been assigned in the region 800-600 cm^{-1} [45]. The vibrations belonging to the bond between the benzene ring and halogen atoms were worth the discussion here, since mixing of several vibrations are possible due to the lowering of the molecular symmetry, and the occurrence of heavy atoms on the periphery of molecule [46]. The present calculations place the Cl-C group stretching modes at 872,856 cm^{-1} in FT-Raman and at 832,815 cm^{-1} in experimental FT-Raman spectrum of the molecule. The computational frequencies were identified in DFT at 831,801 cm^{-1} and 785, 713 cm^{-1} (HF) are assigned to Cl-C stretching vibration show good agreement with the earlier literature [47].

4.4 Nonlinear optical properties

Nonlinear optics properties 3C3'MS were calculated using the density functional theoretical method. Nonlinear optical properties deal with the interaction of applied electric fields with different materials. The effect is established as generation of new electric fields that differ in phase, altered in frequency, amplitude or other physical properties [48]. The theoretical calculations have been shown to be useful in the description of the structure–property relationship between the polarizability and hyperpolarizabilities characterize the response of a molecular system in an applied electric field [49]. The theoretical methodology allows the determination of NLO properties as an inexpensive way to design molecules by studying their potential before synthesis and to determine the electronic structure and vibrational contributions to the high order hyperpolarizability of the molecular structure. Theoretical study plays an important role in understanding the molecular property relationship which is able to assistance in designing novel NLO materials. Theoretically, calculated values of polarizability (α) and hyperpolarizability (β) are shown in Table (4a) and (4b). The highest values of first hyperpolarizability (β_{tot}) ($2.705X10^{-24}$) is obtained in the method of HF/6-311++G (d, p) level using GAUSSIAN 09W package. It is interesting to note that the first hyperpolarizability of the title compound is twenty times that of the standard NLO material urea (0.13×10^{-30} esu) [50].

Table4 (a) Polarizability α_{tot}(x10^{-24}esu) of the 3C3'MS molecule calculated at the DFT and HF method of 6- 311++G (d, p) level.

*	DFT	HF
α_{xx}	-95.4172	-98.2402
α_{xy}	12.8560	14.9773
α_{yy}	-97.7730	-98.4713
α_{xz}	-0.0146	-0.0133
α_{yz}	-0.0012	-0.0030
α_{zz}	-111.9262	-115.0013
α	1.507X10^{-23}	1.525X10^{-23}
Δα	2.292X10^{-24}	2.705X10^{-24}

Table 4 (b) Hyperpolarizability β (x10^{-31}esu) of the 3C3'MS molecule calculated at the DFT and HF method of 6- 311++G (d, p) level.

*	DFT	HF
β_{xxx}	-277.8612	-291.9696
β_{xxy}	30.1117	31.3506
β_{xyy}	9.0819	9.2730
β_{yyy}	2.4885	2.3886
β_{xxz}	0.0575	0.0351
β_{xyz}	-0.0232	-0.0216
β_{yyz}	-0.0105	-0.0186
β_{xzz}	-3.1948	0.0351
β_{yzz}	0.0055	0.0809
β_{zzz}	0.0165	0.0243
β_{ii}	2.366X10^{-30}	2.459X10^{-30}

4.5 UV-Vis Spectra Analysis

Time-dependent density functional theory (TD-DFT) calculation has been performed for 3C3'MS on the basis of completely optimized ground state molecular structure to investigate the electronic properties. The Molecules allow strong π–π* and σ –σ* electron transition in the UV-Vis range with high extinction coefficients. UV spectra analyses of 3C3'MS have been studied by computational method [51]. In order to recognize electronic transitions of the molecule, TD-DFT calculations on electronic absorption spectra in the different solvent (Acetonitrile, Methanol, Ethanol) were performed. The calculated results involving the frontier orbital energies, oscillator strengths (*f*), absorption wavelengths (λ) and excitation energies (E) for different solvent (Acetonitrile, Methanol, Ethanol) phase are illustrated in Table (5a) and (5b) and the UV-Vis spectra of 3C3'MS is shown in Fig. 6. TD-DFT calculations expect three transitions in the near ultraviolent region for 3C3'MS molecule. As it can be seen from the UV–Vis spectra [52], absorption maximum values have been found to be 202, 241, 316 nm for Acetonitrile, 209, 241, 303 nm for Methanol, and 305,240, 206 nm Ethanol solution at TD-DFT/6-311++G (d, p) lavel theory. The absorption band of 3C3'MS at the longer observed peak at 316 nm is caused by the π–π* transition. Except for 316 nm, all the other absorption bands are mostly derived due to the observed transition from HOMO-LUMO is π–π*.

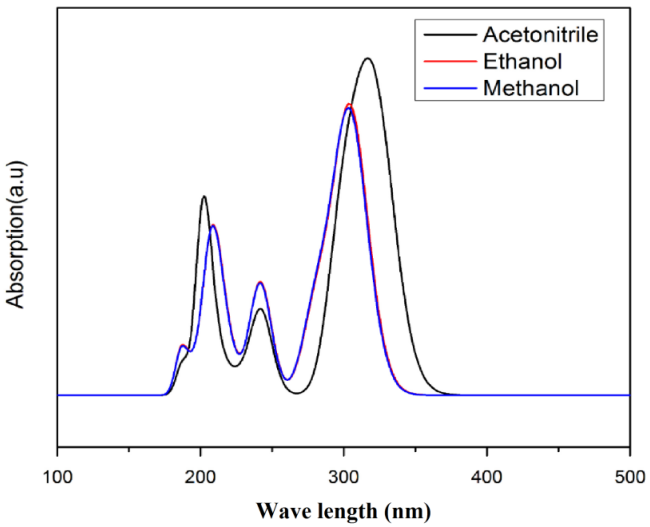

Fig. 6 Simulated UV absorption spectra.

Table 5 (a) Computed excitation energies, electronic transition configurations and oscillator strengths (f) for the

Solvent	Configurations composition (corresponding Transition orbitals)	Excitation Energy (eV)	Wave length (nm)	Oscillator Strength (f)
Acetonitrile	63→65 64 → 65	3.85	321	0.5011
	63→65 64 → 65 64 → 67	4.124	300	0.0006
	62→ 65 63→ 66 64→66	4.56/	271	0.0093
Ethanol	63→ 65 64→ 65	4.07	304	0.7479
	63→ 65 64→ 65 64→ 67	4.40	281	0.2559
	62→65 63→ 66 64→ 66	4.60	269	0.0019
Methanol	63→ 65 64 → 65	4.07	304	0.7348
	63 → 65 64 → 65 64 → 67	4.40	281	0.2599
	62 → 65 63 → 66 64 → 66	4.60	269	0.0020

Table 5 (b) Calculated Maximum absorption wavelength (λ_{max}), Oscillator Strength (f), Excitation energy (eV) and Corresponding Electronic Transition for 3C3'MS.

Excited state	Wavelength λ (nm)	Excitation energy (cm^{-1})	Oscillator strength (f)	Major contributions
Acetonitrile	31097	321.5	0.7433	H->L (90%) H-1->L (9%)
	33265	300.6	0.5011	H-1->L (85%), H->L (10%)
	36853	271.3	0.0006	H-1->L (85%), H->L (10%)
	40888	244.5	0.0093	H-3->L (35%), H-2->L (58%)
	41357	241.7	0.2147	H-2->L (36%), H->L+1 (48%)
Ethanol	32852	304.4	0.7479	H->L (94%)
	35517	281.5	0.2559	H-1->L (83%)
	37143	269.2	0.0019	H-2->L (49%), H->L+1 (43%)
	40738	245.4	0.0048	H-3->L (48%), H-2->L (40%)
	41378	241.6	0.2903	H-2->L (32%), H->L+1 (46%)
Methanol	32894	304.0	0.7348	H ->L (94%)
	35537	281.3	0.2599	H-1->L (82%)
	37146	269.2	0.0020	H-2->L (49%), H->L+1 (43%)
	40749	245.4	0.0045	H-3->L (45%), H-2->L (42%)
	41396	241.5	0.2872	H-2->L (32%), H->L+1 (47%)

4.6 Molecular Electrostatic Potential

The MEP are useful 3D plots that can be used to visualize atomic charge distributions and charge related properties of studied compound, MEP surface map was computed at DFT/6-311++G (d, p) optimized geometries. These maps are used as a reactivity displaying most possible sites for nucleophilic and electrophilic attacks. There are useful in biological application and non-covalent interactions particularly hydrogen bonds interactions [53, 54]. The surface is related to the molecular stability and is a very useful descriptor for determining the sites for electrophilic and nucleophilic reactions, the study of biological recognition processes and hydrogen bonding interactions. In addition, they provide information on the atomic charge related properties and atomic charge distribution of molecules. The MESP is an important parameter, and their study leads to a better understanding of complex biological processes involving the dipole–dipole, charge–dipole, and quadruple–dipole interactions. The electron total density onto which the molecular electrostatic surface map has been displayed in Figs. 7a and 7b, the electron density isosurface being 0.002 a.u. Figure reveals that negative regions (blue) are mostly localized over the O atoms for the electrophilic attack and the positive regions (green) are mainly localized in the Cl-atoms for a nucleophilic attack.

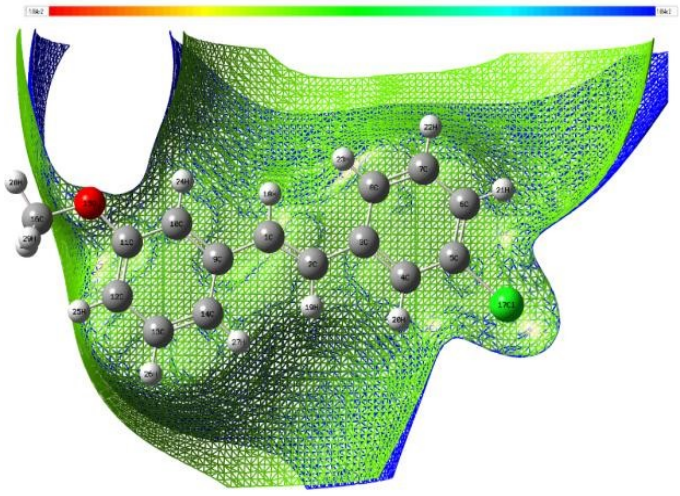

Fig. 7a Electrostatic potential contour map.

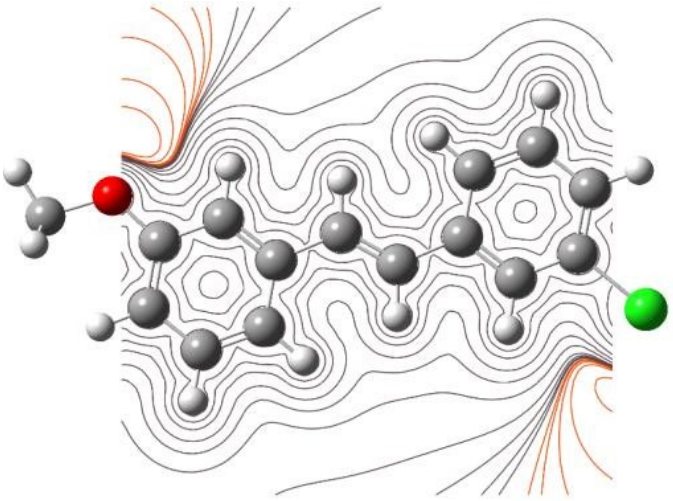

Fig. 7b Electrostatic potential contour map.

4.7 Natural Bonding Orbital's

NBO analysis is a useful tool to investigate the highest possible percentage of the electron density between occupied Lewis-type (donor (i)) NBOs are thereby complemented by the unoccupied non-Lewis type (acceptor (j)) NBOs within the molecular system [55]. The delocalization effects can be recognized from the off-diagonal NBO Fock matrix elements of the second order Perturbation theory analysis. The interaction between occupancies of the bonding and weak occupancies of the valence anti-bonding molecular orbital energies can be qualitatively described in terms of NBO method that is expressed by means of second-order perturbation interaction energy $\boldsymbol{E^2}$ [55, 56]. In addition, Lewis-type (i) and non-Lewis type (j), the stabilization energy $\boldsymbol{E^2}$ associated with i / j delocalization can be estimated as follows [56]:

$$E^2 = \Delta E_{ij} = q_i \frac{F(i,j)^2}{\varepsilon_i - \varepsilon_j} \qquad (1)$$

Where q_i is the Lewis-type occupancy, ε_i and ε_j are diagonal elements and $F(i,j)^2$ is the off diagonal NBO Fock matrix elements. The interaction between the $F(i,j)^2$ donor- acceptor and NBO Fock matrix elements [56, 57].

4.7.1 Second order Perturbation theory analysis: Donor-accepter interactions

The i - j interactions are considered by analyzing viable interactions between filled Lewis and empty non-Lewis NBOs, after approximating their molecular orbital energies through NBOs analysis. These energetic interactions are termed to as 'delocalization' corrections to the accurate possible natural Lewis structure. The potency of these delocalization interactions are relational to the NBO interacting intensities and molecular orbital energies which give important facts on the interactions among various parts of the molecules [58-60]. Some significant orbital intramolecular hyper-conjugative interactions and corresponding NBO energies derived from the second order perturbation computation are listed in Table 6, which shows the most significant interactions between Lewis and non-Lewis orbital with C and O lone pairs.

The intra-molecular interaction is formed by the orbital overlap of bonding between σ (C-C) and antibonding σ*(C-C) orbital, which results that intramolecular charge (ICT) is causing stabilization of the system.NBO analysis has been performed on the 3C3'MS molecule at the DFT/6-311++G (d, p) level in order to elucidate, the intra-molecular rehybridization and delocalization of electron density within the molecule. The most important conjugative interactions in the title molecule involving lone pair LP(1) of O15 with σ*(C11-C12), σ*(C11-C12), and of σ* (C5-C6) with the same result in the stabilization 9.53,6.56 and 29.01 kcal/mol, respectively, and also the lone pair LP(2) of the O15 with σ*(C11-C12) with the stabilization energy of 6.56 kcal/mol. As evident from Table 6, the hyperconjugative interaction due to the orbital overlap between σ bonding orbitals of σ(2)C3-C4, σ (2)C7-C8 ,σ(2)C9-C10 and σ* anti-bonding σ*(2)C5-C6,σ*(2)C3-C4 σ*(2) C11-C12 orbitals also results in the intra-molecular charge transfer contributing to stabilization of the molecular system [61].

Table 6. Second order perturbation theory analysis of Fock matrix of 3C3'MS by NBO method by DFT/6-311++G (d, p) method.

Donor (i)	Acceptor (j)	E(2)[a] kcal/ mol	E(j)-E(i) [b] a.u.	F(i,j)[c] a.u.
σ(2)C1-C2	π(3)C9	0.58	0.96	0.022
σ(2)C1-C2	σ*(2)C3-C4	13.71	0.29	0.060
σ(2)C3-C4	σ*(2)C5-C6	23.28	0.26	0.069
σ(2)C3-C4	σ*(2)C7-C8	18.48	0.27	0.065
σ(2)C5-C 6	σ*(2)C3-C4	19.17	0.29	0.068
σ (2)C7-C8	σ*(2)C3-C4	20.19	0.28	0.068
σ(2)C9-C10	σ*(2)C11-C12	23.21	0.26	0.071
CR (1)C14	π*(2)C9	1.69	11.22	0.123
nLP (2)O15	σ*(1)C5-C6	9.53	0.32	0.054
nLP (1)O15	σ*(1)C11-C12	6.56	1.10	0.076
nLP (2)O15	σ*(2)C11-C 12	29.01	0.32	0.092
σ*(2)C3-C4	σ*(2)C1-C2	64.23	0.02	0.064
σ*(2)C5-C6	σ*(2)C3-C4	228.3	0.01	0.080
σ*(2)C11-C12	σ*(2)C 9 - C 10	262.1	0.01	0.081

LR→ lone pair.

[a] Stabilisation (delocalisation) energy.

[b] Energy difference between i (donor) and j (acceptor) NBO orbitals.

[c] Fock matrix element i and j NBO orbitals.

4.8 Mulliken Atomic Charges

The natural population charge calculation plays an important role in the application of theoretical calculation to molecular structures [62], because the atomic charges affect the electronic structure, polarizability, and much more properties of the molecular systems. The Mulliken charge distributions of the title molecule have been calculated by methods DFT/6-311++G (d,p) and HF/6-311++G(d,p) methods with 6-311++G (d, p) levels of theory are collected in Table 7 and the better represent in graphical chart form as given Fig. 8. From the results, It is worthy to mention that C5, C11 and Cl17 atoms of 3C3'MS exhibit more positive charges than other H atoms in an aromatic ring and carbon atoms substituted by chloride group have highest atomic charges, while the O15

atom in the molecule have negative charges which form the C3, C6 and C9 atoms. The greater electro-negative (ionic) character of negative charge on O atom and positive charge on Cl atom may suggest the formation of intermolecular bonding interaction in solid forms.

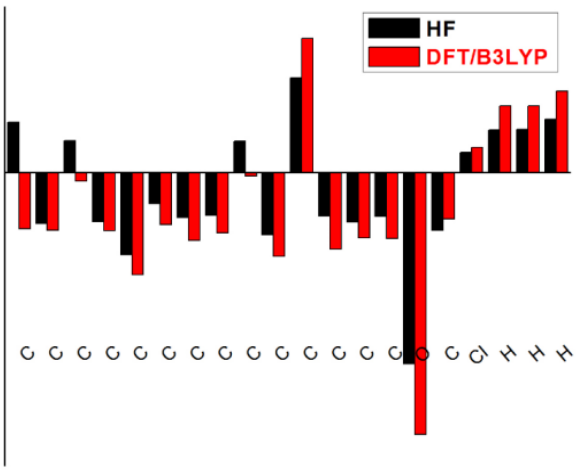

Fig. 8 Mulliken population analysis chart.

Table 7 Mulliken atomic charge analysis of 3C3'MS.

Atoms	Atomic charge (Z_A)	
	DFT	HF
C1	0.14848	-0.16586
C2	-0.15002	-0.16995
C3	0.09345	-0.02588
C4	-0.14415	-0.17174
C5	0.24273	0.30057
C6	-0.09192	-0.15322
C7	-0.13293	-0.20061
C8	-0.12662	-0.17687
C9	0.09242	-0.01098
C10	-0.18336	-0.24651
C11	0.27876	0.39479
C12	-0.12752	-0.22523
C13	-0.14593	-0.19343
C14	-0.12971	-0.19495
O15	-0.56349	-0.77017
C16	-0.16982	-0.13623
CI17	0.05863	0.07367
H18	0.12574	0.19628
H19	0.12629	0.19665

4.9 Molecular properties

The HOMO and LUMO energy values are useful descriptors in studying global reactivity of molecules and chemical hardness (*h*), chemical potential (μ), electronegativity (χ), electrophilicity index (ω) and softness (*S*). The chemical Hardness (*h*) is defined within the computational method as the total energy (E) with respect to the number of electrons (*N*) as external potential *V(r)* property of the system that measures both the global descriptors and molecular stability of the molecules [63].

$$\eta = \left[\frac{\partial^2 E}{\partial N^2}\right]_{V(r)} \quad (2)$$

Using Koopman's theorem for closed-shell molecules [64], ionization potential (*IP*), electron affinity (*EA*), chemical potential, chemical hardness and softness, electrophilicity index as well as electronegativity defined [65]. The HOMO and LUMO orbital energies as IP and EA are related to the energy values of the E_{HOMO} and E_{LUMO} can be expressed as:

$$IP = -E_{HOMO} \quad (3)$$

$$EA = -E_{LOMO} \quad (4)$$

$$\eta = \frac{IP-EA}{2} \quad (5)$$

$$S = \frac{1}{\eta} \quad (6)$$

Where IP and EA, Chemical Hardness (η) and softness (S) [66] are known as global reactivity descriptors [67, 68] and have been theoretically justified within the background of DFT and TD-DFT [64]. These chemical descriptors-based parameters are commonly used to measure chemical reactivity and molecular properties [69]. Chemical hardness basically deals with the physical polarization of the electron cloud of the ions or molecules and atoms under small perturbation during a molecular properties and chemical reactivity [70]. Generally, soft molecules have a smaller value and the hard molecules have a larger E_{HOMO} and E_{LUMO} energy gap value [71, 72]. The computed values of the hardness, softness, chemical potential, electronegativity, and electrophilicity index, IP of donor and EA of acceptor have been calculated and the results are presented in Table 1.

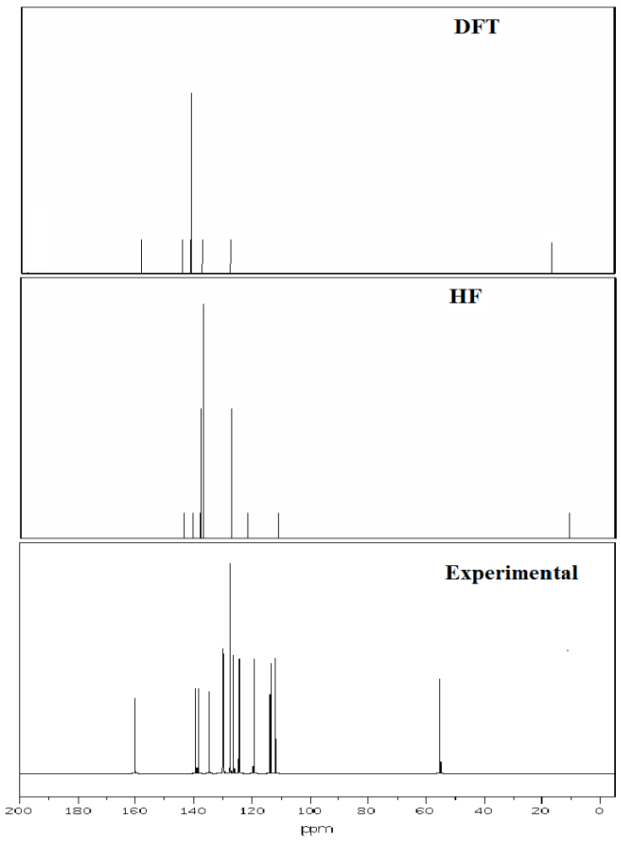

Fig. 9 Experimental and theoretical ^{13}C NMR spectra.

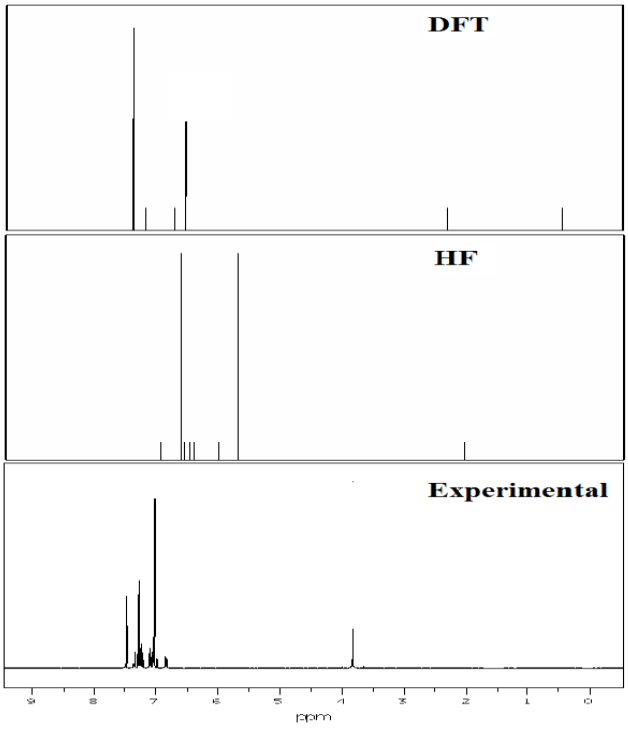

Fig. 10 Experimental and theoretical ^{1}H NMR spectra.

4.10 NMR Spectra analysis

The theoretical values for ^{1}H and ^{13}C NMR Chemical shift of 3C3'MS have been compared with the excellent agreement with experimental data are listed in Table 8. The structural parameters are obtained with the DFT and HF/6-311++ G (d, p) level of theory and it is used to predict ^{1}H and ^{13}C chemical shifts with the recommended GIAO approach [73] and TMS is used for reference. The experimental and theoretical NMR spectra of the 3C3'MS molecule is shown in Figs. 9 and 10 respectively. Aromatic carbon peaks are observed from 160.01 to 56 ppm and calculated values by DFT and HF methods range from 156 to 17 and 142 to 12 ppm. The carbon atoms C16, C12, C14, C10, C8, C6, C13 and C3 are recognized to downfield NMR signals 160.01,141,139,136,130,130 and 128. These reveal the presence of partially positive charge on the carbon atoms [74]. The chemical shift (δ) value provides information on the chemical environment/magnetic properties of the protons. Protons next to electron donating groups are shielded and protons next to electron withdrawing groups are deshielded [75]. The proton numbered H30 has the maximum chemical shift value 7.5 ppm. The 30H to 27H downfield is observed in the experimental values in ^{1}H with respect to calculated values. All computations are in good agreement with experimental data.

Table 8 NMR Chemical shift (^{13}C and ^{1}H) of 3C3'MS [δ (ppm)].

Atoms	Experimental	DFT	HF
16C	160	156	142
12C	141	142	140
14C	139	140	138
10C	136	140	137
8C	130	138	131
6C	130	138	122
13C	128	130	114
3C	56	17	12
30H	7.5	7.5	7.0
24H	7.3	7.5	6.8
20H	7.3	7.3	6.7
21H	7.2	7.2	6.6
25H	7.1	6.8	6.5
26H	7.0	6.7	6.5
19H	3.8	2.4	5.8
27H	-	0.6	1.9

4.11 Natural Charge Analysis

Natural charges and electron population charge analysis [76] have been important role in the application of density functional calculation of molecular system. The difference of charge magnitude is in proportion with the natural charges, but they differ appreciably because this analysis includes number of core, valance and Rydberg electrons located in diffuse orbital. The development of atomic charges on the separate atom and the accumulation of electrons in the valance, core and Rydberg sub-shells are shown in Table 9. In the most electronegative charge of 0.52278 is accumulated on the oxygen atom O6 and -0.23811is accumulated on the carbon atom C4. Usually the electron cloud between bonded atoms is symmetrical, when the two atoms are similar but if one of atoms has a greater tendency to attract the electron cloud then it shifts slightly towards that atom. According to an electrostatic point of new of the molecule, these electronegative atoms have a tendency to donate an electron. Whereas, the most electropositive atoms such as; H10 have a tendency to accept an electron [77]. Further, the natural population analysis showed that 128 electrons in the 3C3'MS molecule is distributed on the sub shells as follows:

Core: 41.98304 (99.9596% of 42)

Valance: 85.81491 (99.7848% of 86)

Rydberg: 0.20205 (0.1579% of 128)

Table 9. Natural Population analysis of 3C3'MS

Atoms	Charge (e)	Natural population (e)			Total (e)
		Core	Valence	Rydberg	
C_1	-0.19571	1.99898	4.18647	0.01026	6.19571
C_2	-0.21423	1.99897	4.20489	0.01036	6.21423
C_3	-0.05348	1.99893	4.04248	0.01208	6.05348
C_4	-0.23811	1.99878	4.2282	0.01113	6.23811
C_5	-0.01624	1.99843	4.00026	0.01754	6.01624
O_6	-0.52278	1.99972	6.51755	0.00551	8.52278
C_7	-0.3559	1.99927	4.34998	0.00666	6.3559
Cl_8	-0.04686	9.99981	7.04005	0.00701	17.04686
H_9	0.22932	0.0073	0.76918	0.0015	0.77068
H_{10}	0.23071	0.0002	0.76783	0.00146	0.76929

4. 12 Thermodynamic analysis

Thermodynamic analysis is important for understanding the chemical processes. The theoretical calculation is a well-established and efficient tool to calculate various statistical thermodynamic properties of molecular system. Nowadays, due to theoretical predictions of thermodynamic properties, and their experimental measurements are possible with high accuracy. The thermodynamic functions such as enthalpy change, heat capacity and molar entropy can be predicted easily from the molecular partition function. These calculations are used to convert molecular energy levels into macroscopic properties. Molecular energy arises from electronic excitation, Molecular translation, rotation, and vibration. This information establishes the spectroscopy of the molecule of interest [78, 79]. In the present studies, the parameters such as SCF energies, specific heat capacities, rotational constants, zero-point vibrational energies, dipole moments, rotational temperatures, 3C3'MS have been calculated at DFT and HF method with 6-311++G(d,p) basis set are listed in Table 10.

Table 10. Theoretically computed zero-point vibrational energy (Kcal mol^{-1}), rotational constants (GHz), rotational temperatures (Kelvin), thermal energy (Kcal mol^{-1}), molarcapacity at constant volume (cal mol^{-1} $Kelvin^{-1}$), dipole moment (Debye) and vibrational temperatures (Kelvin) for 3C3'MS.

Parameter	DFT/B3LY	HF
Zero-point vibrational energy	150.66513	160.36038
Rotational constant (GHZ)	1.41876	1.41876
	0.12322	0.12322
	0.11345	0.11345
Rotational temperature (Kelvin)	0.06809	0.06809
	0.00591	0.00591
	0.00544	0.00544
Energy total (KCal/Mol)	160.108	168.481
Translational(KCal/Mol)	0.889	0.889
Rotational(KCal/Mol)	0.889	0.889
Vibrational(KCal/Mol)	158.331	166.704
Dipole moment	3.7721	3.7290
Vibrational temperature (Kelvin)	11.21	90.53
	70.14	129.94
	78.14	164.14
	99.35	219.61
	142.91	251.23
	225.55	258.08
	267.41	315.80
	285.17	338.57
	290.92	416.53
	336.66	433.71
	362.21	439.60
	380.06	493.59
	434.12	511.64
	460.29	597.74
	566.91	629.37
	639.98	686.24
	654.65	763.73
	677.52	785.62

5. CONCLUSIONS

In this study, comparing the theoretical FT-IR, FT-Raman and Experimental FT-IR, FT-Raman spectra of the title compound 3C3'MS have been recorded. The investigations on fundamental modes along with structural, thermodynamic, electronic analysis, Natural population analysis and Mulliken population analysis of the compound have been made using ab initio DFT and HF methods with 6-311++G(d,p) basis sets. Close agreement is observed in the molecular geometries like bond lengths and bond angles calculated by DFT and HF methods. The UV-Vis spectra analysis of the molecule was also carried out. Theoretical ^{13}C and ^{1}H chemical shift values are reported and compared with experimental data, showing a very good agreement both for ^{13}C and ^{1}H. The HOMO–LUMO energy gap helped in analyzing the chemical reactivity of the molecule. Global hardness, softness and electrophilicity were calculated. The FMOs have been pictured and the HOMO–LUMO energy gap has been calculated. First hyperpolarizability analysis reveals that the title compound possesses considerable NLO properties. The NBO analysis have been made with which the chemical stability and intra molecular interactions have been interpreted and the transactions give stabilization to the structure have been identified by second order perturbation energy calculations. The ESP map shows that the negative potential sites are on oxygen as well as the positive potential sites are the hydrogen and chlorine atom in a molecule.

ABBREVIATIONS

3C3'MS 3-Chloro-3'-Methoxystilbene
RHF Restricted Hartree-Fock
MP2 Moller-Plesset second order perturbation theory
NMR Nuclear Magnetic Resonance
ICT Intramolecular change transfer
HOMO Highest occupied molecular orbital
LUMO Lowest unoccupied molecular orbital
DFT Density Functional Theory
IVR Intramolecular Vibrational Redistribution

ACKNOWLEDGEMENTS

The authors are thankful to the learned referees for their useful and critical comments, which improved the quality of the manuscript. One of the authors, M. Prakasam, acknowledges Periyar University for financial support in the form of a University Research Fellowship (URF).

REFERENCE

[1] J. Saltiel, J. D.Agostino, E. D. Megarity, L. Metts, K. R. Neuberger, M. Wrighton, O. C. Zafiriou, O.L. Chapman, The cis-trans Photoisomerization of Olefins Marcel Dekker, New York, 1973.
[2] D. H. Waldeck, Chem. Rev. 1991, 91, 436. View Article
[3] H. Meier, Angew. Chem. Int. Ed. Engl. 1992, 31, 1540. View Article
[4] J. S. Baskin, L. Banares, S. Pedersen, A. H. Zewail, J. Phys. Chem. 1996, 100, 11933. View Article
[5] P. Senthilkumar, C. Nithya and P. M. Anbarasan. J. Mol. Mod. 2013, 19, 4573. PMid:23959394 View Article PubMed/NCBI
[6] K.A. Muszkat, Top. Curr. Chem. 1980, 88, 143
[7] T. Nakabayashi, H. Okamoto, M. Tasumi, J. Phys. Chem. 1998, 102, 9695 View Article
[8] S. L. Schultz, J. Qian, J.M. Jean, J. Phys. Chem. 1997, 101, 1006. View Article
[9] R. J. Sension, A. Z. Szarka, R.M. Hochstrasser, J. Chem. Phys. 1992, 97, 5242. View Article
[10] J. K. Rice, A. P. Baronavski, J. Phys. Chem. 1992, 96, 3366. View Article
[11] H. Sanei, A. Asoodeh, S. Hamedakbari-Tusi, J. Chamani, J Solu. Chem. 2011, 40, 1905. View Article
[12] P. Mokaberi, V. Reyhani, Z. Amiri-Tehranizadeh, M. R. Saberi, S. Beigoli, F. Samandar and J. Chamani, New J Chem. 2019, 43, 8132. View Article
[13] Z. Sharif-Barfeh, S. Beigoli, S. Marouzi, A. Sharifi Rad, A. Asoodeh, J. Chamani, J. Sol. Chem. 2017, 46, 488. View Article
[14] M. Zolfagharzadeh, M. Pirouzi, A. Asoodeh, M.R. Saberi and J. Chamani, J. Biomol. Struc. Dynam. 2014, 32, 1936. PMid:24125112 View Article PubMed/NCBI
[15] J. Grundy, Chem. Rev. 1957, 57, 356. View Article
[16] K. Hagiwara, N. Kosaka, Y. Yoshioka, R. Takahashi ,F. Takeshita & T. Ochiya, Sci. Rep. 2012, 2, 314. PMid:22423322 View Article PubMed/NCBI
[17] H. A. Ali, K. Kondo, Y. Tsuda, Chem. Pharm. Bull. 1992, 40, 1136.
[18] H. Matsuda, N. Tomohiro, K. Hiraba, S. Harima, S. Ko, K. Matsuo, M. Yoshikawa, M. Kubo, Bio. Pharm. Bull. 2001, 24, 267. PMid:11256482 View Article PubMed/NCBI
[19] S. Sanoh, S. Kitamura, K. Sugihara, N. Fujimoto, S. Ohta, J. Heal. Sci. 2003, 49, 367. View Article
[20] K. Tsumura, K. Furuya, A. Sakamoto, Mo. Tasumi, J. Raman Spectrosc. 2008, 39, 1591. View Article
[21] A. Weigel, N. P. Ernsting, J. Phys. Chem. B 2010, 114, 7893. PMid:20481560 View Article PubMed/NCBI
[22] R. K. Chaudhuri, J. Phys. Chem. A 2013, 117, 9434. PMid:23530611 View Article PubMed/NCBI
[23] A. L. Houk, I. L. Zheldakov, T. A. Tommey, and C. G. Elles, J. Phys. Chem. B 2015, 119, 9344. PMid:25369524 View Article PubMed/NCBI
[24] M. Arivazhagan, V. Krishnakumar, J. Xavier, G. Ilango, V. Balachandran, Spectrochimi. Acta Part A 2009, 72, 946. PMid:19196545 View Article PubMed/NCBI
[25] R. G.W .Yang, Density Functional Theory of Atoms and Molecular, Oxford, New York, 1989.
[26] R. O .Jones, O. Gunnarson, Rev.Mol.Phys. 1989, 61, 689 View Article
[27] T. Ziegier, Chem. Rev. 1991, 91, 651. View Article
[28] W. Kohn, L. J .Sham, Phys. Rev. A 1965, 140, 1133. View Article
[29] A. D. Becke, Phys. Rev. Part A 1988, 38, 3098 PMid:9900728 View Article PubMed/NCBI
[30] C .T. Lee, W.T. Yang, R.G. Parr, Phys. Rev. Part B. 1988, 37, 785. PMid:9944570 View Article PubMed/NCBI
[31] J. Frisch, G.W. Trucks, H.B .Schlegel, G.E .Scuseria, M.A. Robb, J.R .Cheeseman, H. Nakatsuji, M. Caricato, X. Li, H.P. Hratchian, K. Toyota, R. Fukuda, J. Hasegawa, M. Ishida, R. Nakajima, Y. Honda, O. Kilao, H. Nakai, T. Verven, J. A. Montgomery Jr., J. E .Peralta, F. Ogliaro, M .Bearpark, J.J .Heyd, E. Brothers, K. N. Kudin, V. N. Staroveror, R. Kobayashi, J. Normand, K. Ragavachari, A .Rendell, J. C. Burant, S .J. Tomasi, M .Cossi, N. Rega, J.M .Millam, M. Klene, J .E Knox, J .B. Cross, V. Bakken, C. Adamo, J. Jaramillo, R. Gomperts, R .E. Strattmann, O .Yazyev, A.J. Austin, R. Cammi, J.W. Ochetrski, R.L. Martin, K. Morokuma, V. G. Zakrazawski, G .A. Votn, P. Salvador, J.J. Dannenberg, S. Dapprich, A.D. Daniels, O. Farkas, J. B. Foresman, Gaussian O. G., Revision A.O2 Gaussian Inc., Wallingford, CT, 2009.
[32] A. D .Becke, J. Chem. Phys. 1993, 98, 5652. View Article
[33] C. Lee, W. Yang, R. C .Parr, J. Phys. Rev. B 1998, 37, 789.
[34] T. Sundius, J. Mol. Struct. 1990, 218, 326. 80287-T

View Article
[35] Computer program Gauss View 3.09, Ver. 2 Gaussian Inc, PA, Pittsburgh, 2008.
[36] P. Pulay, G. Fogarasi, F. Pang, J. E. Boggs, J. Am. Chem. Soc. 1979, 10, 2550. View Article
[37] G. Keresztury, J.M. Chalmers, P.R. Griffth, Raman Spectroscopy: Theory in Handbook of Vibrational Spectroscopy, John Wiley & Sons Ltd., New York, 2002.
[38] M.S. Alam, D .U. Lee, J. Mol. Struc. 2017, 1128, 185.
[39] M. Bakiler, I.V. Maslov, S. Akyuz, J. Mol. Struct. 1999, 475, 83. 00491-8 View Article
[40] J. S. Murray, K .Sen, Elsevier, Amsterdam, the Netherlands, 1996.
[41] J. Chamani, M. Heshmati, J Coll. Interf. Sci. 2008, 322, 119. PMid:18405913 View Article PubMed/NCBI
[42] V. Krishnakumar, N .Prabavathi, Spectrochim. Acta Part A 2009, 72, 747. PMid:19121975 View Article PubMed/NCBI
[43] G.Varsanyi, Academic Kiaclo, Budapest, 1973.
[44] P.S. Kalsi, Sectroscopy of Organic Compounds New Age International P Limited Publishers, New Delhi, 2005.
[45] V. Balachandran, G. Santhi, V. Karpagam, A. Lakshmi, Spectrochim. Acta Part A 2013, 110, 140. PMid:23562743 View Article PubMed/NCBI
[46] R. A. Yadav, I .S .Sing, Indian J. Pure Appl. Phys. 1985, 23, 627.
[47] K. Parimala, V. Balachandran, Spectrochim. Acta Part A 2011, 81, 723. PMid:21795105 View Article PubMed/NCBI
[48] Y. R. Shen, the Principles of Nonlinear Optics Wiley, New York, 1984.
[49] P. Vennila, M . Govindaraju, G .Venkatesh, C . Kamal, J. Mol. Struct. 2016, 1111, 156. View Article
[50] M. Adant, L. Dupuis, L .Bredas, Int. J. Quantum Chem. 2004, 56, 507.
[51] B. M. Wong, M. Piacenza, F. Della Sala, Phys. Chem. Chem. Phys. 2009, 11, 4508. PMid:19475168 View Article PubMed/NCBI
[52] A.A. Moosavi-Movahedi, J. Chamania, M. Gharanfoli, G.H. Hakimelahi, Thermochimica Acta, 2004, 409, 137.